Spin Defects in hBN assisted by Metallic Nanotrenches for Quantum Sensing

Hongbing Cai, Shihao Ru, Zhengzhi Jiang, John Jun Hong Eng, Ruihua He, Fu-Li Li, Yansong Miao, Jesús Zúñiga-Pérez, Weibo Gao

Spin Defects in hBN assisted by Metallic Nano-trenches for Quantum Sensing

Hongbing Cai[1, 2, #], Shihao Ru[1, 3, #], Zhengzhi Jiang[1], John Eng Jun Hong[1], Ruihua He[4], Fuli Li[3], Jesús Zúñiga-Pérez[1,5]*, Weibo Gao[1, 2, 5, 6]*

[1]*Division of Physics and Applied Physics, School of Physical and Mathematical Sciences, Nanyang Technological University, Singapore 637371, Singapore.*

[2]*The Photonics Institute and Centre for Disruptive Photonic Technologies, Nanyang Technological University, Singapore 637371, Singapore*

[3]*School of Physics, Xi'an Jiaotong University, Xi'an 710049, China*

[4] *School of Biological Sciences, Nanyang Technological University, Singapore 637551, Singapore*

[5]*MajuLab, International Research Laboratory IRL 3654, CNRS, Université Côte d'Azur, Sorbonne Université, National University of Singapore, Nanyang Technological University, Singapore, Singapore*

[6]*Centre for Quantum Technologies, National University of Singapore, Singapore 117543, Singapore.*

Abstract: The omnipresence of hexagonal boron nitride (hBN) in devices embedding two-dimensional materials has prompted it as the most sought platform to implement quantum sensing due to its testing-while-operating capability. The negatively charged boron vacancy (V_B^-) in hBN plays a prominent role, as it works at room-temperature, can be easily generated and, most importantly, its spin population can be initialized and read out by optical means. But its low quantum yield hinders its widespread use as an integrated quantum sensor. Here, we demonstrate an emission enhancement amounting to 400 by metallic nanotrench arrays compatible with coplanar waveguide (CPW) electrodes employed for spin-state detection. By monitoring the reflectance spectrum of the resonators as additional layers of hBN are transferred, we have optimized the overall hBN/nanotrench optical response, maximizing thereby the luminescence enhancement. Based on these finely tuned heterostructures, we achieved an enhancement of DC magnetic field sensitivity, attaining a highest sensitivity of $6\times10^{-5}\ T/Hz^{1/2}$.

Keywords: hexagonal boron nitride (hBN), negatively charged boron vacancy (V_B^-) defects, Tunable plasmonic, quantum sensing, optically detected magnetic resonance (ODMR)

Addressable solid-state single photon emitters (SPEs) in bulk materials such as diamond[1, 2], gallium nitride[3], and silicon carbide[4], have shown brilliant performance in a broad range of applications going from quantum networks and quantum computation to quantum sensing[5, 6, 7]. However, one of the key challenges limiting their practical use is their relatively low emission intensity, whose enhancement would ease further their applicability. In this sense, many efforts have been made to enhance both the emission and collection efficiency of quantum emitters. Compared to bulk materials, the emerging layered 2D materials are natural candidates attaining more efficient coupling with plasmonic nanostructures and photonic nanocavities due to their inherent "thin" 2D scale[8, 9, 10, 11, 12], which imposes a unique vertical location of the emitters.

Among the various 2D materials that can hold SPEs, hexagonal boron nitride (hBN) covers a wide range of emission wavelengths going from the ultraviolet to the infrared region, and has a relatively mature material platform[13]. Many methods have been developed to generate SPEs on hBN monolayers or flakes, such as direct synthesis[14, 15], ion implantation[16, 17, 18], strain engineering[19, 20], e-beam irradiation[21, 22, 23], and thermal annealing[24]. Several reports have revealed that SPEs in hBN are spin manipulable and that, in particular, negatively charged boron vacancy (V_B^-) defects can be easily generated and their spin population can be controlled at room temperature[25, 26, 27, 28, 29, 30, 31, 32, 33]. Although V_B^- defects have been utilized in proof-of-principle quantum sensors over the last three years, their broader application necessitates boosting their emission intensity. Recently, a few groups have developed different methods to enhance the V_B^- emission in layered hBN, all of them demonstrating an emission enhancement with respect to the bare substrate[34, 35, 36]. However, all these methods ignored the effect of the hBN thickness on the resonance behavior of the photonic structures, which can dramatically affect the actual emission enhancement and, potentially, also the emitter's emission stability.

In this work we demonstrate that nanotrench arrays (NTAs) are efficient plasmonic structures

enabling the enhancement of the emitters' photoluminescence (PL) intensity by orders of magnitude whenever the emitter and photonic mode of the overall structure are spectrally matched. To achieve it, the photonic mode is tuned in-situ by the subsequent transfer of additional hBN layers until the resonance of the combined hBN/nanotrench resonator meets the emission wavelength of V_B^- defects. Moreover, this NTA structure is compatible with coplanar waveguide electrodes, which improves the sensitivity for measuring DC magnetic fields.

As shown in Fig. 1a, the V_B^- defects in the thin hBN layer are located below the surface at a depth *Di*. At the same time, the plasmonic mode in the metallic nanostructures has a maximum working distance of Hp[18]. Based on the electric field distribution simulation results shown in Fig.1b and 1c, it is observed that the maximum enhancement of electric field intensity occurs near the interface of the gold film and hBN layer, and decreases rapidly with increasing thickness of the hBN flake. From this perspective, along the vertical direction the target emitters should be located as close as possible to the metal surface. However, direct contact between the emitters and the metal film will cause the quenching of their emission, so a certain thickness of a decoupling material is necessary for the plasmonic device to operate efficiently. Here we use the nanotrench array to enhance the emission intensity of the V_B^- defects by modulating the plasmonic mode of these metallic nanostructures, which are located only below the emitters. As shown in scanning electron microscopy (SEM) image (Fig S1), a typical nanotrench array with a gap size of 20 nm, depth of 150 nm, and pitch length of 300 nm is directly fabricated on 200 nm thick coplanar waveguide electrodes by focused ion beam (FIB) milling. From the PL spectrum measured in Fig 1e (Fig. S2 for magnified PL spectrum of the defects on bare SiO_2 substrate), an average enhancement factor (EF) of about 400 is realized on the nanotrench array compared to the signal from the V_B^- defects on the bare SiO_2 substrate,

and an enhancement factor of ~15 compared to the defect's emission from a flat gold film.

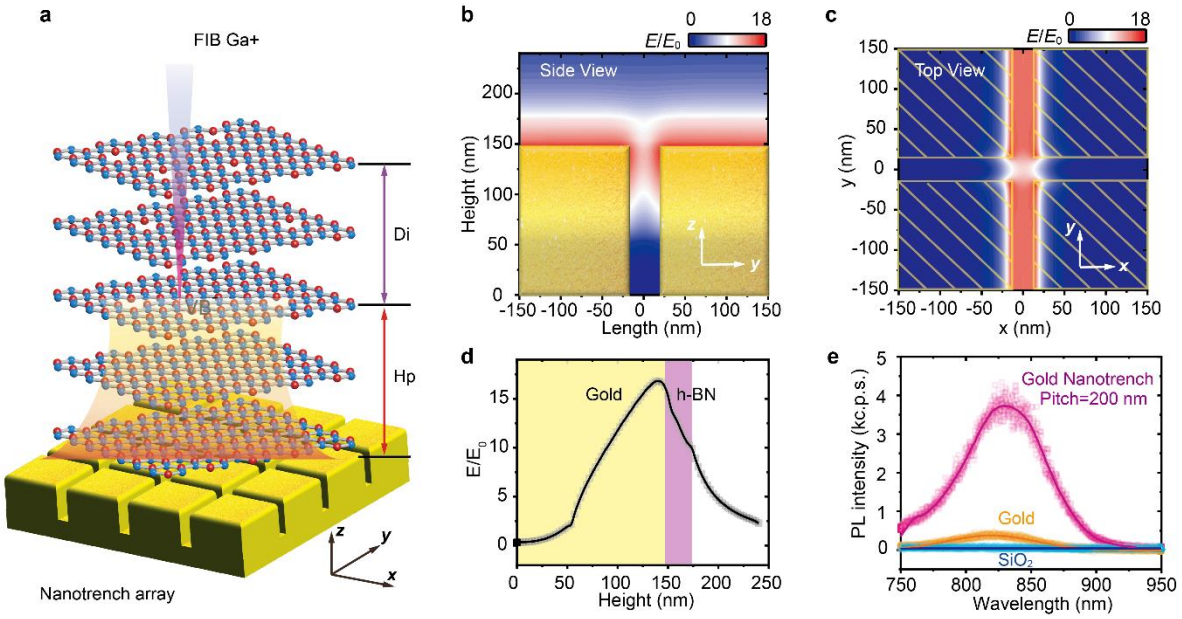

Figure 1 | Design of plasmonic structures to enhance the spin defects in Ga^+ ion implanted hBN thin layer. **a,** The coupling principle for the spin defects in hBN with the plasmonic mode on gold nanotrench array. **b, c,** Simulated electric field distribution in the nanotrench area (side-view) and 5-nm above the surface of the hBN/nanotrench heterostructure. The electrical field of incident light is polarized parallelly to x-axis. **d,** Height dependence of the field enhancement at x=0 in the hBN/nanotrench heterostructures. **e,** PL spectrum on different substrates shows the emission enhancement of the plasmonic nanotrench.

In order to get the largest coupling efficiency of the hBN layer and the plasmonic structures, the resonant wavelength of the Au nanotrench should match the emission energy of the V_B^- defects. However, the transfer of hBN dramatically changes the resonant wavelength of the nano grooves array and introduces a spectral mismatch between the hBN/nanotrench resonator and the V_B^- emission wavelength, deteriorating the emitter/resonator coupling. In the following we demonstrate how to exploit the resonators sensitivity to the hBN thickness deposited thereon to finely tune in-situ the actual resonant wavelength. We start by designing nanotrench arrays with different pitches ranging from 200 nm to 500 nm while keeping the same gap width

of ~20 nm. From the simulation results shown in Fig. S3a, we can find that the resonant peaks of the nanotrenches shift from 660 nm to 830 nm as a function of the pitch. Based on the simulation results we fabricated the associated nanotrench arrays, which reproduce the calculated reflectance spectra in Fig. S3b. Under these conditions (i.e. without hBN on top of the resonators) the nanotrench array with periods of 500 nm, with a resonant wavelength of ~832 nm, matches best the emission wavelength of V_B^- defects, which peaks at about 830 nm. However, after the transfer of the hBN thin layer, with a thickness of just 10 nm, the resonant wavelength of all the nanotrench arrays shows a dramatic redshift, as shown in Fig. S3c. This observation gives us a chance to in-situ tune the resonant wavelength of the plasmonic nanostructures by simply stacking the optimum number of hBN layers. To illustrate the effect of this approach, different layers of hBN were transferred onto the 250 nm pitch nanotrench array sequentially, as schematically shown in Fig. 2, and optical measurements were carried out after every layer transfer. Each transferred layer of hBN has a similar thickness of about 10 nm. From the measured reflectance spectra plotted in Fig. 2a-c and Fig. S4, we find that the resonant wavelength can be modulated across an extensive wavelength range from 720 nm to 1050 nm, which agrees well with the simulated result shown in Fig. 2d-f.

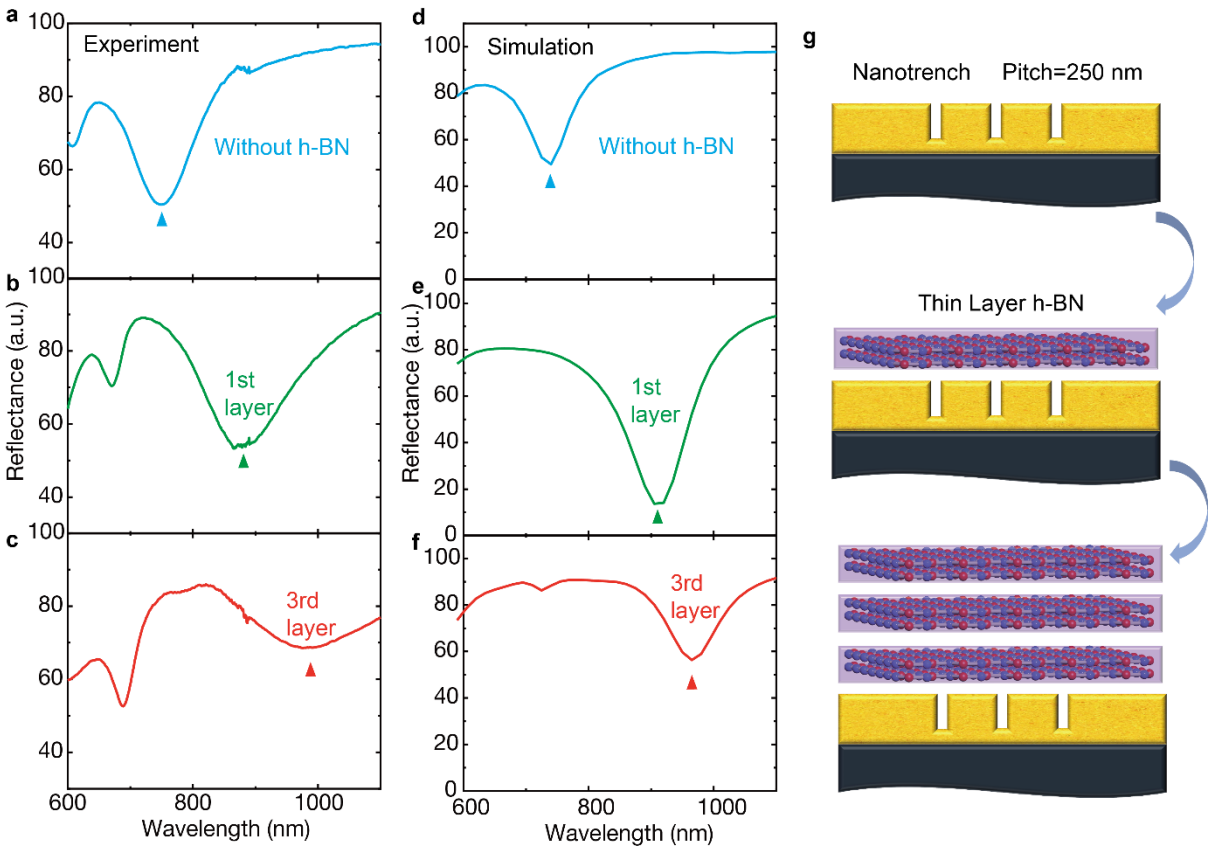

Figure 2 | Thickness engineering of resonance mode in hBN/nano-trench plasmonic heterostructures. a-c, Measured reflectance spectra for the 250 nm pitch nanotrench array without hBN; after transfer of one thin layer and three thin layers. **d-f,** Simulated reflectance spectra for the corresponding heterostructures plotted in Fig. a-c. **g,** Schematics illustration of the transfer of thin layers of hBN (~10 nm thick each) to tune the resonant wavelength of the heterostructures.

Next, we studied the enhancement capability of the nanotrench array. Since the wavelength changes strongly upon the transfer of hBN, we expect a strong dependence of the enhancement factor as the resonator comes on and off resonance with the emission of the V_B^- defects. Fig. 3b presents the PL intensity mapping for the implanted hBN transferred onto the nanotrench arrays with different pitches as shown in Fig. 3a. Their reflectance spectra before the hBN transfer were described in Fig. 2a and S3. We note first that due to the existence of gap plasmon modes all the nanotrench arrays do enhance the emission of V_B^- emitters compared to bare silica as

well as flat gold substrate, where only localized surface plasmons can be expected. Besides, it is clear that the nanotrench array that matches the resonant wavelength of defects at 830 nm reaches the maximum enhancement factor. As shown in Fig. 3c and 3d, the brightest emission comes from the nanotrench array with a pitch of 200 nm, whose resonant wavelength is localized at about 830 nm after the transfer of hBN (see figure S3c), which matches perfectly the emission wavelength of V_B^- defects in hBN. In contrary, although the resonant wavelength of the nanotrench with the pitch of 500 nm matches the emission wavelength of hBN at 830 nm before the transfer of hBN, after the transfer of hBN its emission is strongly red-shifted and the final enhancement is much lower. We also measure the lifetime dependence of the PL spectrum for the V_B^- defects at different areas and find out that the emitters at the 200 nm pitch nanotrench show a slightly decreased lifetime (~2), as shown in Fig. S5. In contrast, the other emitters have a similar lifetime. Overall, this shows that either the emission is still dominated by non-radiative defects or the time-resolved measurements reflect the lifetime of the majority of the emitters, which lie on top of the gold film and not on the trenches. This last explanation is also consistent with the fact that the average PL enhancement (figure 3d) is much smaller than the actual enhancement within the nanotrenches, which can be computed by considering the surface ratio between the trenches (where the gap plasmon mode enhances the emission) and the unstructured gold (where only localized surface plasmon modes contribute to the enhancement).

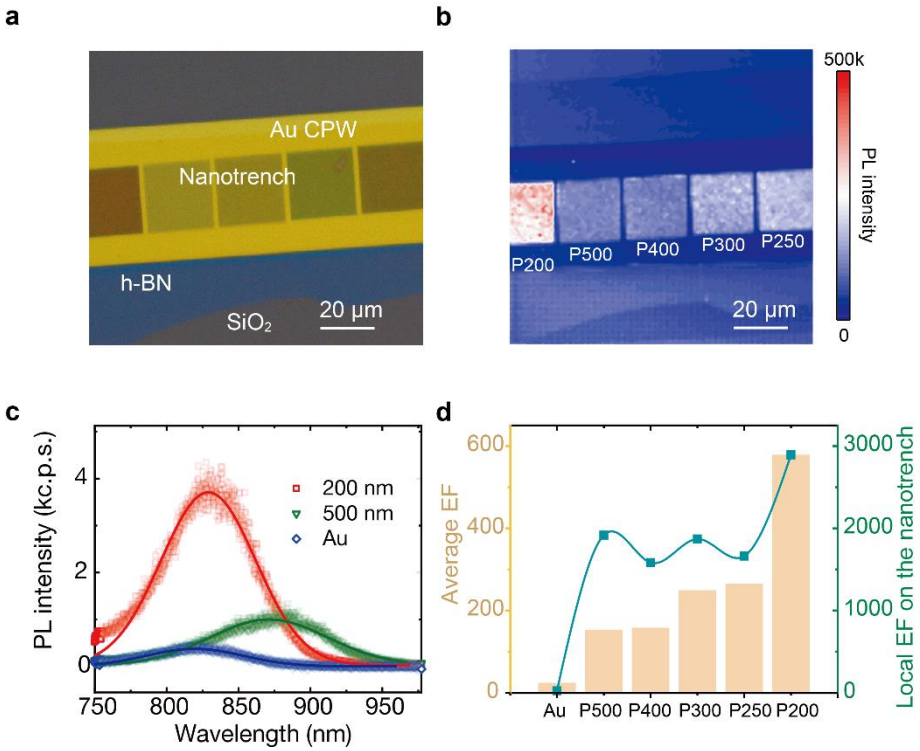

Figure 3 | PL enhancement of hBN emitters nano-trench patterns with different pitches. a, Optical microscope image for the Ga+ implanted hBN transferred onto the nanotrench array with different pitches on the gold CPW electrodes. **b,** PL intensity mapping for the spin defects emitters on the nanotrench array with different pitches. **c,** PL spectrum for the spin defects emitters in hBN on different nanotrench arrays, which shows the most significant enhancement factors are more than 40 times compared with the signal on flat gold film. The PL spectra also show a red shift in peak position and intensity reduction due to the plasmonic resonant wavelength change. **d,** The average enhancement factor (EF) and local EF for different nanotrench arrays. Note that for the local enhancement we have considered that all trenches contribute to the enhancement and, thus, we do not make any assumption on the actual emitter dipole.

After successfully stacking hBN layers to modulate the resonant wavelength of hBN/nanotrench resonators and establishing the conditions for optimum coupling, we turn to evaluate its sensing performances. The setup and measurement scheme for spin modulation are described in Methods. The plasmonic nanostructures described in this work offer the advantage of being compatible with coplanar waveguide electrodes, as illustrated in Fig. 4a. The V_B^- defect in hBN has a triplet ground state and a triplet excited state. Its spin modulation signals

can be readout because of the spin-dependent intersystem crossing. Fig. 4b displays a typical measurement sequence of optically detected magnetic resonance (ODMR). We can obtain ODMR signals in both the nanotrench structure and the flat gold film, with discrete ODMR signals for $m_s = \pm 1$ thanks to the Zeeman splitting under magnetic field. The experimental ODMR results are shown in Fig. 4c, with a laser power of 6.5 mW, -10 dBm input microwave power, and identical integration times. Even though the coupling of microwave to the hBN on nanotrench is lower, leading to a decreased ODMR contrast, the PL signal of V_B^- defects on nanotrench is 40 times larger than that on Au, resulting in a better signal-to-noise ratio. From the ODMR spectra, the sensitivity of DC magnetic field can be calculated for Lorentzian shapes as $\eta_{DC} \sim \frac{4}{3\sqrt{3}} \frac{h}{g_e \mu_B} \frac{\Delta\nu}{C\sqrt{I}}$, where h and μ_B are Planck constant and Bohr magneton constant, respectively. $\Delta\nu$, C, I are the linewidth (FWHM), contrast and detected signal strength of the measurements.[37,38] By varying the laser power while keeping the microwave power fixed, we investigated the sensitivity of the DC magnetic field as a function of the laser power, as illustrated in Fig. 4d. By optimizing the laser and microwave power, we achieved a DC magnetic field sensitivity of ~ $6\times10^{-5}\ T/Hz^{1/2}$, which is comparable to the best performance reported for V_B^- defects in a hBN thin layer[5,6].

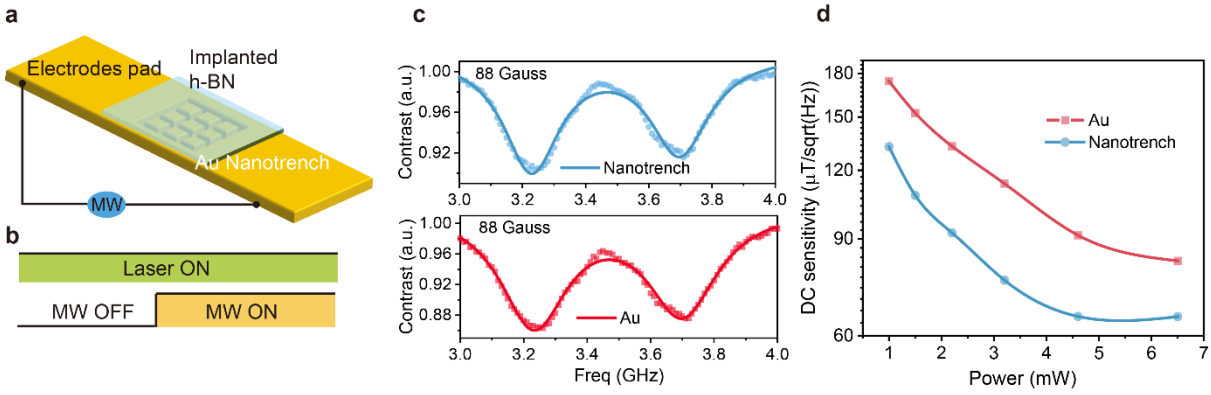

Figure 4 | Quantum sensing using the nanotrench/hBN heterostructures. a, Schematic illustration of a metallic nanotrench array on the coplanar waveguide electrodes. **b,** The typical ODMR measurement sequence

for the V_B^- defects. **c,** The ODMR signal of the V_B^- defects under a small magnetic field. **d,** The DC sensitivities of the V_B^- defects on flat gold and nanotrench array as a function of microwave power.

In conclusion, by engineering the thickness of the deposited hBN, we have demonstrated the in-situ modulation of the resonant mode of hBN/nanotrench array heterostructures, necessary to match the emission energy of the V_B^- defects in hBN. The reflectance spectrum characterization revealed that adding a top hBN layer can shift the resonant wavelength of the heterostructures from the visible to infrared range, thus modifying strongly the photonic response of the complete system. Upon optimization of the hBN thin layer thickness, we achieved an average PL intensity enhancement factor of 40 as compared to bare gold film. Furthermore, we presented the feasibility of integrating the plasmonic heterostructures into the CPWs and the DC sensitivity can be enhanced to reach ~ $6\times10^{-5}\ T/Hz^{1/2}$, the best value obtained by hBN. The in-situ modulation of the resonant wavelength for plasmonic nanostructures in this work may be applied to any other layered material, potentially opening new ways to control in-situ the light-matter interaction in 2D devices.

■ASSOCIATED CONTENT

Supporting Information

The Supporting Information is available free of charge at https://pubs.acs.org/doi/xx.xxx/acs.nanolett.xxxxxx.

Methods on sample preparation, SEM characterization of the fabricated nanotrench array, Reflectance spectra for nanotrench array with different pitches, ODMR, Peak shift of the nanotrench after transfer of different layer of hBN, Lifetime measurement of the defects on nanotrench with different pitches. (PDF)

■AUTHOR INFORMATION

Corresponding Authors

Jesús Zúñiga-Pérez − Division of Physics and Applied Physics, School of Physical and Mathematical Sciences, Nanyang Technological University, 637371, Singapore; MajuLab, International Research Laboratory IRL 3654, CNRS, Université Côte d'Azur, Sorbonne Université, National University of Singapore, Nanyang Technological University, 637371, Singapore; Email: jesus.zuniga@ntu.edu.sg

Weibo Gao − Division of Physics and Applied Physics, School of Physical and Mathematical Sciences, Nanyang Technological University, 637371, Singapore; The Photonics Institute and Centre for Disruptive Photonic Technologies, Nanyang Technological University, 637371, Singapore; Centre for Quantum Technologies, National University of Singapore, 117543, Singapore; orcid.org/0000-0003-3971-621X; Email: wbgao@ntu.edu.sg

Authors

Hongbing Cai − Division of Physics and Applied Physics, School of Physical and Mathematical Sciences, Nanyang Technological University, 637371, Singapore; The Photonics Institute and Centre for Disruptive Photonic Technologies, Nanyang Technological University, 637371, Singapore; orcid.org/0000-0003-3186-1041

Shihao Ru − Division of Physics and Applied Physics, School of Physical and Mathematical Sciences, Nanyang Technological University, 637371, Singapore; School of Physics, Xi'an Jiaotong University, Xi'an 710049, China; orcid.org/0000-0002-5119-0452

Zhengzhi Jiang − Division of Physics and Applied Physics, School of Physical and Mathematical Sciences, Nanyang Technological University, 637371, Singapore

John Eng Jun Hong − Division of Physics and Applied Physics, School of Physical and Mathematical Sciences, Nanyang Technological University, 637371, Singapore

Ruihua He − School of Biological Sciences, Nanyang Technological University, Singapore 637551, Singapore;

Fuli Li − School of Physics, Xi'an Jiaotong University, Xi'an 710049, China.

Author Contributions

All authors contributed extensively to the manuscripts.

Author Contributions

HB. Cai. and SH. Ru. contributed equally.

Notes

The authors declare no competing financial interest.

■ACKNOWLEDGMENTS

This work is supported by the Singapore National Research Foundation through QEP programme (No. NRF2021-QEP2-03-P01, No. NRF2021-QEP2-03-P10) and Singapore Ministry of Education (MOE2016-T3-1-006 (S)).

■REFERENCES

1. Zhou Y, Rasmita A, Li K, Xiong Q, Aharonovich I, Gao W-b. Coherent control of a strongly driven silicon vacancy optical transition in diamond. *Nature Communications* 2017, **8**(1)**:** 14451.

2. Chen D, Fröch JE, Ru S, Cai H, Wang N, Adamo G*, et al.* Quantum Interference of Resonance Fluorescence from Germanium-Vacancy Color Centers in Diamond. *Nano Lett* 2022, **22**(15)**:** 6306-6312.

3. Zhou Y, Wang Z, Rasmita A, Kim S, Berhane A, Bodrog Z*, et al.* Room temperature solid-state quantum emitters in the telecom range. *Science Advances* 2018, **4**(3)**:** eaar3580.

4. Mu Z, Zargaleh SA, von Bardeleben HJ, Fröch JE, Nonahal M, Cai H*, et al.* Coherent Manipulation with Resonant Excitation and Single Emitter Creation of Nitrogen Vacancy Centers in 4H Silicon Carbide. *Nano Lett* 2020, **20**(8)**:** 6142-6147.

5. Gottscholl A, Diez M, Soltamov V, Kasper C, Krauße D, Sperlich A*, et al.* Spin defects in hBN as promising temperature, pressure and magnetic field quantum sensors. *Nature Communications* 2021, **12**(1)**:** 4480.

6. Huang M, Zhou J, Chen D, Lu H, McLaughlin NJ, Li S*, et al.* Wide field imaging of van der Waals ferromagnet Fe3GeTe2 by spin defects in hexagonal boron nitride. *Nature Communications* 2022, **13**(1)**:** 5369.

7. Lyu X, Tan Q, Wu L, Zhang C, Zhang Z, Mu Z*, et al.* Strain Quantum Sensing with Spin Defects in Hexagonal Boron Nitride. *Nano Lett* 2022, **22**(16)**:** 6553-6559.

8. Liu Y, Fang H, Rasmita A, Zhou Y, Li J, Yu T*, et al.* Room temperature nanocavity laser with interlayer excitons in 2D heterostructures. *Science Advances* 2019, **5**(4)**:** eaav4506.

9. Luo Y, Shepard GD, Ardelean JV, Rhodes DA, Kim B, Barmak K*, et al.* Deterministic coupling of site-controlled quantum emitters in monolayer WSe2 to plasmonic nanocavities. *Nature Nanotechnology* 2018, **13**(12)**:** 1137-1142.

10. Yang L, Xie X, Yang J, Xue M, Wu S, Xiao S*, et al.* Strong Light–Matter Interactions between Gap Plasmons and Two-Dimensional Excitons under Ambient Conditions in a Deterministic Way. *Nano Lett* 2022, **22**(6), 2177–2186.

11. Turunen M, Brotons-Gisbert M, Dai Y, Wang Y, Scerri E, Bonato C*, et al.* Quantum photonics with layered 2D materials. *Nature Reviews Physics* 2022. **4**, 219–236

12. Fröch JE, Kim S, Mendelson N, Kianinia M, Toth M, Aharonovich I. Coupling Hexagonal Boron Nitride Quantum Emitters to Photonic Crystal Cavities. *ACS Nano* 2020, **14**(6)**:** 7085-7091.

13. Mendelson N, Chugh D, Reimers JR, Cheng TS, Gottscholl A, Long H*, et al.* Identifying carbon as the source of visible single-photon emission from hexagonal boron nitride. *Nat Mater* 2021, **20**(3)**:** 321-328.

14. Tran TT, Bray K, Ford MJ, Toth M, Aharonovich I. Quantum emission from hexagonal boron nitride monolayers. *Nature Nanotechnology* 2016, **11**(1)**:** 37-41.

15. Hayee F, Yu L, Zhang JL, Ciccarino CJ, Nguyen M, Marshall AF*, et al.* Revealing multiple classes of stable quantum emitters in hexagonal boron nitride with correlated optical and electron microscopy. *Nat Mater* 2020, **19**(5)**:** 534-539.

16. Ziegler J, Klaiss R, Blaikie A, Miller D, Horowitz VR, Alemán BJ. Deterministic Quantum Emitter Formation in Hexagonal Boron Nitride via Controlled Edge Creation. *Nano Lett* 2019, **19**(3)**:** 2121-2127.

17. Gao X, Pandey S, Kianinia M, Ahn J, Ju P, Aharonovich I*, et al.* Femtosecond Laser Writing of Spin Defects in Hexagonal Boron Nitride. *ACS Photonics* 2021, **8**(4)**:** 994-1000.

18. Guo N-J, Liu W, Li Z-P, Yang Y-Z, Yu S, Meng Y*, et al.* Generation of Spin Defects by Ion Implantation in Hexagonal Boron Nitride. *ACS Omega* 2022, **7**(2)**:** 1733-1739.

19. Proscia NV, Shotan Z, Jayakumar H, Reddy P, Cohen C, Dollar M*, et al.* Near-deterministic activation of room-temperature quantum emitters in hexagonal boron nitride. *Optica* 2018, **5**(9)**:** 1128-1134.

20. Li C, Mendelson N, Ritika R, Chen Y, Xu Z-Q, Toth M*, et al.* Scalable and Deterministic Fabrication of Quantum Emitter Arrays from Hexagonal Boron Nitride. *Nano Lett* 2021, **21**(8)**:** 3626-3632.

21. Gale A, Li C, Chen Y, Watanabe K, Taniguchi T, Aharonovich I*, et al.* Site-Specific Fabrication of Blue Quantum Emitters in Hexagonal Boron Nitride. *ACS Photonics* 2022, **9**(6), 2170-2177.

22. Fournier C, Plaud A, Roux S, Pierret A, Rosticher M, Watanabe K*, et al.* Position-controlled quantum emitters with reproducible emission wavelength in hexagonal boron nitride. *Nature Communications* 2021, **12**(1)**:** 3779.

23. Shevitski B, Gilbert SM, Chen CT, Kastl C, Barnard ES, Wong E*, et al.* Blue-light-emitting color centers in high-quality hexagonal boron nitride. *Phys Rev B* 2019, **100**(15)**:** 155419.

24. Chen Y, Li C, White S, Nonahal M, Xu Z-Q, Watanabe K*, et al.* Generation of High-Density Quantum Emitters in High-Quality, Exfoliated Hexagonal Boron Nitride. *ACS Applied Materials & Interfaces* 2021, **13**(39)**:** 47283-47292.

25. Yu P, Sun H, Wang M, Zhang T, Ye X, Zhou J*, et al.* Excited-State Spectroscopy of Spin Defects in Hexagonal Boron Nitride. *Nano Lett* 2022, **22**(9)**:** 3545-3549.

26. Reimers JR, Shen J, Kianinia M, Bradac C, Aharonovich I, Ford MJ*, et al.* Photoluminescence, photophysics, and photochemistry of the V_B^- defect in hexagonal boron nitride. *Phys Rev B* 2020, **102**(14)**:** 144105.

27. Baber S, Malein RNE, Khatri P, Keatley PS, Guo S, Withers F*, et al.* Excited State Spectroscopy of Boron Vacancy Defects in Hexagonal Boron Nitride Using Time-Resolved Optically Detected Magnetic Resonance. *Nano Lett* 2022, **22**(1)**:** 461-467.

28. Gottscholl A, Diez M, Soltamov V, Kasper C, Sperlich A, Kianinia M*, et al.* Room temperature coherent control of spin defects in hexagonal boron nitride. *Science Advances*, **7**(14)**:** eabf3630.

29. Gao X, Vaidya S, Li K, Ju P, Jiang B, Xu Z*, et al.* Nuclear spin polarization and control in hexagonal boron nitride. *Nat Mater* 2022, **21**(9)**:** 1024-1028.

30. Mu Z, Cai H, Chen D, Kenny J, Jiang Z, Ru S*, et al.* Excited-State Optically Detected Magnetic Resonance of Spin Defects in Hexagonal Boron Nitride. *Phys Rev Lett* 2022, **128**(21)**:** 216402.

31. Stern HL, Gu Q, Jarman J, Eizagirre Barker S, Mendelson N, Chugh D*, et al.* Room-temperature optically detected magnetic resonance of single defects in hexagonal boron nitride. *Nature Communications* 2022, **13**(1)**:** 618.

32. Mathur N, Mukherjee A, Gao X, Luo J, McCullian BA, Li T*, et al.* Excited-state spin-resonance spectroscopy of V_B^- defect centers in hexagonal boron nitride. *Nature Communications* 2022, **13**(1)**:** 3233.

33. Vaidya S, Gao X, Dikshit S, Aharonovich I, Li T. Quantum sensing and imaging with spin defects in hexagonal boron nitride. *arXiv e-prints* 2023**:** arXiv:2302.11169.

34. Xu X, Solanki AB, Sychev D, Gao X, Peana S, Baburin AS*, et al.* Greatly Enhanced Emission from Spin Defects in Hexagonal Boron Nitride Enabled by a Low-Loss Plasmonic Nanocavity. *Nano Lett* 2023, **23**(1) 25–33.

35. Mendelson N, Ritika R, Kianinia M, Scott J, Kim S, Fröch JE*, et al.* Coupling Spin Defects in a Layered Material to Nanoscale Plasmonic Cavities. *Adv Mater* 2022, **34**(1)**:** 2106046.

36. Fröch JE, Li C, Chen Y, Toth M, Kianinia M, Kim S*, et al.* Purcell Enhancement of a Cavity-Coupled Emitter in Hexagonal Boron Nitride. *Small* 2022, **18**(2)**:** 2104805.

37. Wang, Z.; Kong, F.; Zhao, P.; Huang, Z.; Yu, P.; Wang, Y.; Shi, F.; Du, J., Picotesla magnetometry of microwave fields with diamond sensors. Science Advances 2022, **8** (32), eabq8158.

38. Degen, C. L.; Reinhard, F.; Cappellaro, P., Quantum sensing. Reviews of Modern Physics 2017, **89** (3), 035002.

TOC

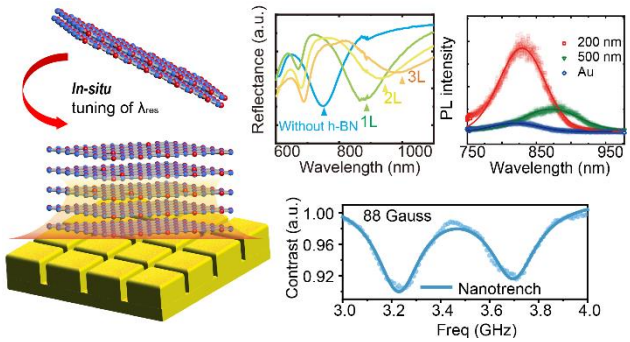
In-situ
tuning of λres
Reflectance (a.u.)
Without h-BN
1L
2L
3L
600
800
1000
Wavelength (nm)
PL intensity
200 nm
500 nm
Au
750
850
950
Wavelength (nm)
Contrast (a.u.)
1.00
0.96
0.92
88 Gauss
Nanotrench
3.0
3.2
3.4
3.6
3.8
4.0
Freq (GHz)